Int J Earth Sci (Geol Rundsch) (2014) 103:801–819
DOI 10.1007/s00531-013-0979-0

ORIGINAL PAPER

Fractures and faults in volcanic rocks (Campi Flegrei, southern Italy): insight into volcano-tectonic processes

Stefano Vitale · Roberto Isaia

Received: 17 May 2013 / Accepted: 29 October 2013 / Published online: 29 November 2013

Abstract The present study was focused to analyze fractures and faults in the Campi Flegrei calderas presently hosting several volcanic edifices, such as lava domes, scoria, and tuff cones. A complex network of fractures and faults affects the volcanic rocks, mostly as planar with highly variable density. Frequently faults appearing as conjugate structures showing normal kinematics often associated with ductile deformation such as drag folds and deflexed layers, suggesting a syn-eruption deformation. However, the most of faults, mainly hosted along the caldera/crater rims, are very steep with dominant normal and secondary reverse movements. The fracture pattern indicates a slight prevalence of NE–SW and NW–SE directions, but N–S and E–W trends also occur. Fractures and faults found in rocks older than 15 ka (Neapolitan Yellow Tuff included), measured in western and eastern sectors of the study area, indicate a rotation of ca. 30° of the main directions among these two sectors. For the faults occurring along the caldera/crater rims, we suggest a kinematic evolution characterized by the reactivation of tensile fractures previously formed in response to both regional extension and locale resurgent dome. Finally, normal faults located in the central sector of caldera, between La Starza and Accademia localities, cutting the youngest volcanic deposits, indicate a constant NNE–SSW extension probably related to the caldera resurgence.

Keywords Campanian Ignimbrite · Neapolitan Yellow Tuff · Caldera · Deformation · Structural geology · Volcanism

Introduction

The Campanian Plain, a Pliocene–Pleistocene graben located in the westernmost sector of the southern Apennines (e.g., Cinque et al. 1993), and its extension in the Tyrrhenian Sea (Gulf of Naples) (Fig. 1), were the location of intense volcanic activity starting from 250 ka and characterized by hundreds of eruptions. The morphology of Campi Flegrei and Bay of Naples mainly results from two large Pleistocene eruptions of the Campanian Ignimbrite (CI) and Neapolitan Yellow Tuff (NYT), and related caldera collapses, followed by many smaller eruptions focused only in the Campi Flegrei area (Di Vito et al. 1999). It is common opinion that all volcanic activities are related to extension following the back-arc opening of the Tyrrhenian Sea (Cosentino et al. 1984; Vitale and Ciarcia 2013). This deformation is testified by pervasive brittle structures, such as tensile fractures and normal faults, affecting all volcanic rocks (e.g., Cosentino et al. 1984; Acocella et al. 1999). A significant increase in studies of volcano-tectonic deformation in Campi Flegrei occurred immediately after the Pozzuoli bradyseismic (slow ground movement) crisis in 1982–1984, calling attention to the non-random pattern of fractures and faults (Cosentino et al. 1984; Calcaterra et al. 1988; Di Vito et al. 1999; Orsi et al. 1999; Acocella

Electronic supplementary material The online version of this article (doi:10.1007/s00531-013-0979-0) contains supplementary material, which is available to authorized users.

S. Vitale (✉)
Dipartimento di Scienze della Terra, dell'Ambiente e delle Risorse (DiSTAR), Università di Napoli Federico II, Largo San Marcellino 10, 80138 Naples, Italy
e-mail: stefano.vitale@unina.it

R. Isaia
Istituto Nazionale di Geofisica e Vulcanologia, Osservatorio Vesuviano, Via Diocleziano 328, 80124 Naples, Italy

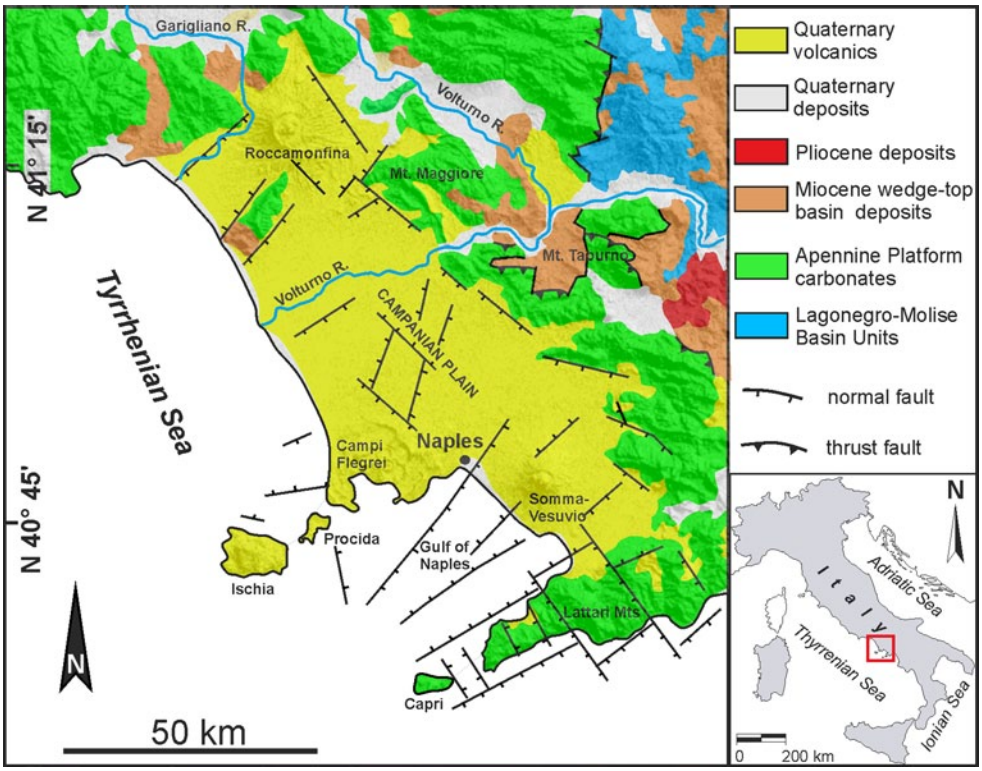

Fig. 1 Geological sketch map of the Campanian Plain (modified from Vitale and Ciarcia 2013; Orsi et al. 1996)

et al. 1999; Acocella 2008, 2010) and suggesting a possible regional stress control on brittle deformation.

This study aims to define the contribution of local versus regional stress field in the deformation history of CF and Napoli area by means of detailed structural analyses of presently fracture network affecting volcanic rocks and clarify the relationships between caldera/crater evolution, fractures and faults.

Geological setting

In this area of Phlegrean Volcanic District (including Campi Flegrei, Procida and Ischia islands, Fig. 1), volcanism started since 200 ka ago. Volcanoclastic successions cropping out in several sectors of the southern Apennines (Rolandi et al. 2003) are the geological record of volcanic activity within the Campanian Plain as old as 250 ka. The Campi Flegrei volcanic field was mainly set up by two caldera collapses following the CI and NYT mayor eruptions. The boundary of these calderas is partly visible on land (Fig. 2) representing also the outer limit for the volcanism younger than 15 ka. Many volcanic edifices variably preserved that were formed by different type eruptions are located within the CI caldera (Fig. 2). These vents range from small scoria cones to tuff ring and tuff cones, with an elevation of more than 300 m a.s.l. (Gauro crater, Fig. 2). The Campi Flegrei volcanism was mainly fed by trachibasaltic to trachytic–phonolitic magmas (Smith et al. 2011 and reference therein) from upper crustal chambers between 8 and 3 km depth (e.g., Arienzo et al. 2010).

The volcanic activity in Campi Flegrei (Fig. 3), as recorded in exposed sections, began in a period prior to 80 ka (Neapolitan volcanoes; Scarpati et al. 2012). In the period between 80 and 39 ka, several volcanic edifices were formed (Fig. 2), including lava and scoria of San Martino, tuff cones of Miliscola and Vitafumo (Monte di Procida), lava domes of Cuma, Punta Marmolite (north of Quarto Plain), and tuff cones of the city of Naples (C.so V.E. di Savoia, Monte Echia and Capodimonte; Rosi and Sbrana 1987; Perrotta et al. 2010; Scarpati et al. 2012). Around 39 ka in Campi Flegrei, the CI eruption occurred (Fisher et al. 1993; Rosi et al. 1996; Civetta et al. 1997; De Vivo et al. 2001), resulting in the largest explosive eruption of the Mediterranean area over the past 200,000 years. More than 300 km^3 of magma and volcanic ash were emitted during this eruption, with deposits extending eastward into Russia (Giaccio et al. 2008; Costa et al. 2012). The magma chamber that fed the eruption was located between 6 and 8 km depth (Marianelli et al. 2006), and its partial depletion led to the formation of the Campi Flegrei caldera (Fig. 2). The caldera margins were the subject of various interpretations in recent literature (e.g., Rosi and Sbrana 1987; Orsi et al. 1996; Perrotta et al. 2006; Acocella 2008) differing mainly in the definition of the eastern sector of the collapsed area, with particular reference to

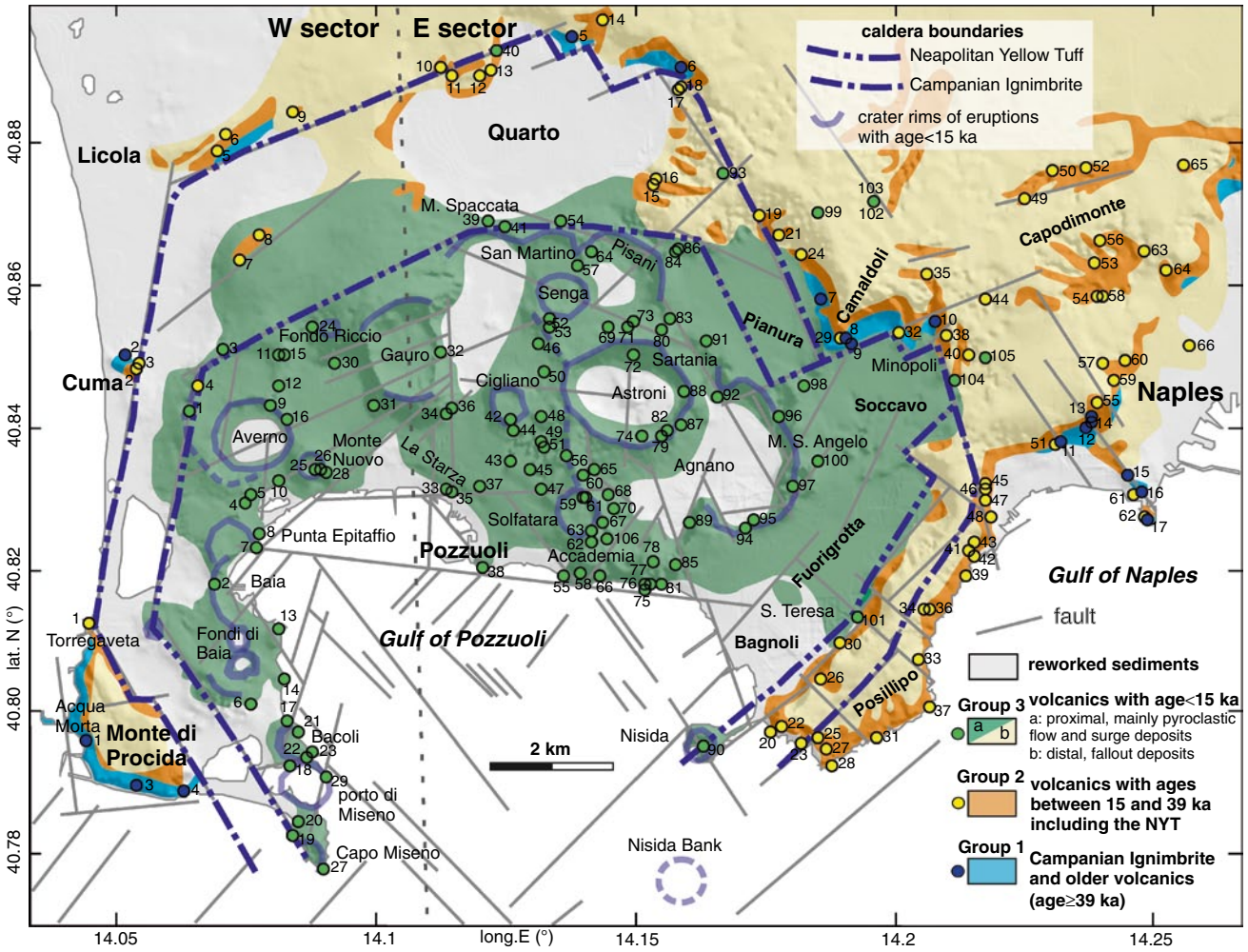

Fig. 2 Simplified geological map of Campi Flegrei and city of Naples including measurement sites (modified after Orsi et al. 1996). The subdivision of *W* and *E sectors* of the analyzed area is shown (*dotted line*). Regional fault traces are inferred by gravimetric lineaments (Florio et al. 1999), morphological structures such as caldera and crater rims and sea seismic profiles (Milia et al. 2000; Bruno et al. 2003; Sacchi et al. 2009). See the supplementary data for names and geographic coordinates of each site

the inclusion or exclusion of the city of Naples in the area affected by the collapse. Some authors (Lirer et al. 1987; Rolandi et al. 2003) exclude the formation of a caldera in relation to the CI eruption, identifying caldera formation at around 15 ka linked to the NYT (Deino et al. 2004) and other previous eruptions (Fig. 3). The NYT eruption was the last dramatic event in the history of the caldera. This phreatoplinian to phreatomagmatic event erupted about 40 km^3 of magma. The tuff, which covered an area of about 1,000 km^2, is generally zeolitized and is commonly used as building material forming the skeleton of the city of Naples. The NYT event led to a further collapse of the Campi Flegrei caldera (Orsi et al. 1992; Scarpati et al. 1993) whose margin is probably exposed only along the eastern edge of the Bagnoli plain (Fig. 2). Likely, this relatively intense eruption reactivated further collapses within the CI caldera.

Following the eruption of the NYT, activity within the caldera generated at least 70 volcanic eruptions (Fig. 3) mainly concentrated in discrete periods alternating with periods of quiescence of variable length (Di Vito et al. 1999; Isaia et al. 2009). The eruption of Monte Nuovo in 1538 A.D. represents the last eruption of the caldera. The volcanic activity of Campi Flegrei was characterized mainly by explosive eruptions with less frequent effusive events. During the last 15,000 years, there have been only two high-magnitude eruptions characterized by Plinian phases (Fig. 3; Agnano-Pomici Principali and Agnano-Monte Spina; Di Vito et al. 1999; De Vita et al. 1999) and medium- and low-magnitude eruptions were predominant. The variability of the events is evidenced by the different areal distributions of deposits and different volumes of magma erupted during eruptions that only for high-magnitude event exceeded 1 km^3 (Orsi et al. 2004; Di Renzo

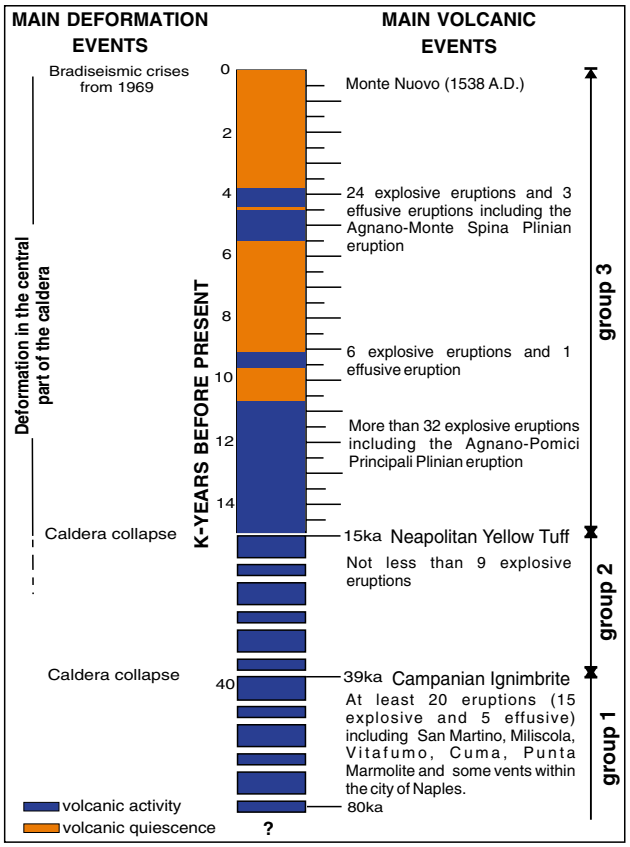

Fig. 3 Schematic time log showing main deformation and volcanic events occurred in Campi Flegrei from 80 ka to the Recent (after Orsi et al. 2004, modified)

et al. 2011). The location of eruptive vents has changed over time, most recently being concentrated in the central-eastern part of the caldera, with respect to the western sector but at least in one case simultaneous eruptions in the two different sectors of the caldera occurred (Isaia et al. 2009; Vilardo et al. 2010).

The caldera was characterized by ground deformation that resulted in a total uplift greater than 100 m in its central part during the last 10,500 years. The main epoch of volcanism was anticipated by resurgence episodes resulting in meters to tens of meters of uplift (Di Vito et al. 1999; Isaia et al. 2009) in response to magma movements at depth. Even over several decades before the Monte Nuovo eruption, ground uplift attained several meters (e.g. Dvorak and Gasparini 1991; Morhange et al. 2006; Guidoboni and Ciuccarelli 2011).

Following the 1538 eruption, Campi Flegrei entered a phase of subsidence that continued until 1950 (Del Gaudio et al. 2010). Recently, slow ground movement (bradyseism) occurred in this area, with two major bradyseismic crises (1970–1972 and 1982–1984) accompanied by an increase in seismicity and 3.5 m of ground uplift (Barberi et al. 1984, 1989; Berrino et al. 1984), forcing the partial evacuation the town of Pozzuoli (Fig. 2). Short-term episodes of uplift, with a cumulative vertical displacement of few tens of cm for each event, have occurred in the last 30 years and are currently underway. On the dynamics of the unrest episodes, many geophysical and geochemical data were produced and discussed (see among others Orsi et al. 1999; Battaglia et al. 2006; Bodnar et al. 2007; Vilardo et al. 2010; Chiodini et al. 2012). The migration of magmatic or hydrothermal fluids as triggering factor for this unrest episode is still debated, as well as the structural pattern that favored the degassing and deformation of the central sector of the caldera. The widespread fumarolic and hydrothermal activity, the historic eruption of Monte Nuovo, and the recent bradyseismic crises are the main volcanic phenomena indicating that the magmatic system of Campi Flegrei remains active.

Fig. 4 Some examples of fractures in volcanic rocks. **a**–**b** Two nearly orthogonal fracture sets in a well-lithified ash layers at Acquamorta and Monte di Procida cliff (*group 1*), respectively. **c** Meter-sized spaced fractures in massive NYT, Torregaveta (*group 2*). **d** Fracture filled by hydrothermal cement in Agnano-Monte Spina ash layers, Solfatara1 (*group 3*). **e** Variable fracture density in different lithified layers, Trentaremi deposits (*group 2*), Lido Pola1. **f** *Cooling joints* in lava deposits, Accademia (*group 3*). **g** *Fracture* related to a ring *fault* bounding the Agnano caldera in *Monte Sant'Angelo deposits* and moderately *NE*-dipping fractures in Solfatara deposits, Pisciarelli1

Structural analyses

All volcanic rocks were divided into three main groups according to their ages: rocks older than 39 ka including the CI (group 1); rocks with ages ranging between 39 and 15 ka and encompassing the NYT (group 2); rocks younger than 15 ka (group 3). Volcanic rocks in the study area are characterized by a complex network of mesoscale fractures and faults (Figs. 4, 5, 6, 7). More than 8,000 attitudes of planar structures were collected at 189 outcrops (see supplementary data) spread over Campi Flegrei and city of Naples (Fig. 2). Because of intense urbanization, most of available outcrops are located along the coastline, in quarries, in tunnels and caves, in protected areas such as natural reserves and archeological sites, and finally in preserved outcrops framed between old and new buildings.

Fractures and faults

Most of fractures (>90 %) are steeply dipping (dip >60°; Fig. 8) with apertures up to a maximum of 30 cm, locally filled with volcanic or hydrothermal deposits (e.g., Figs. 4d, 5e, 6g). Generally fractures, in well-bedded deposits, are

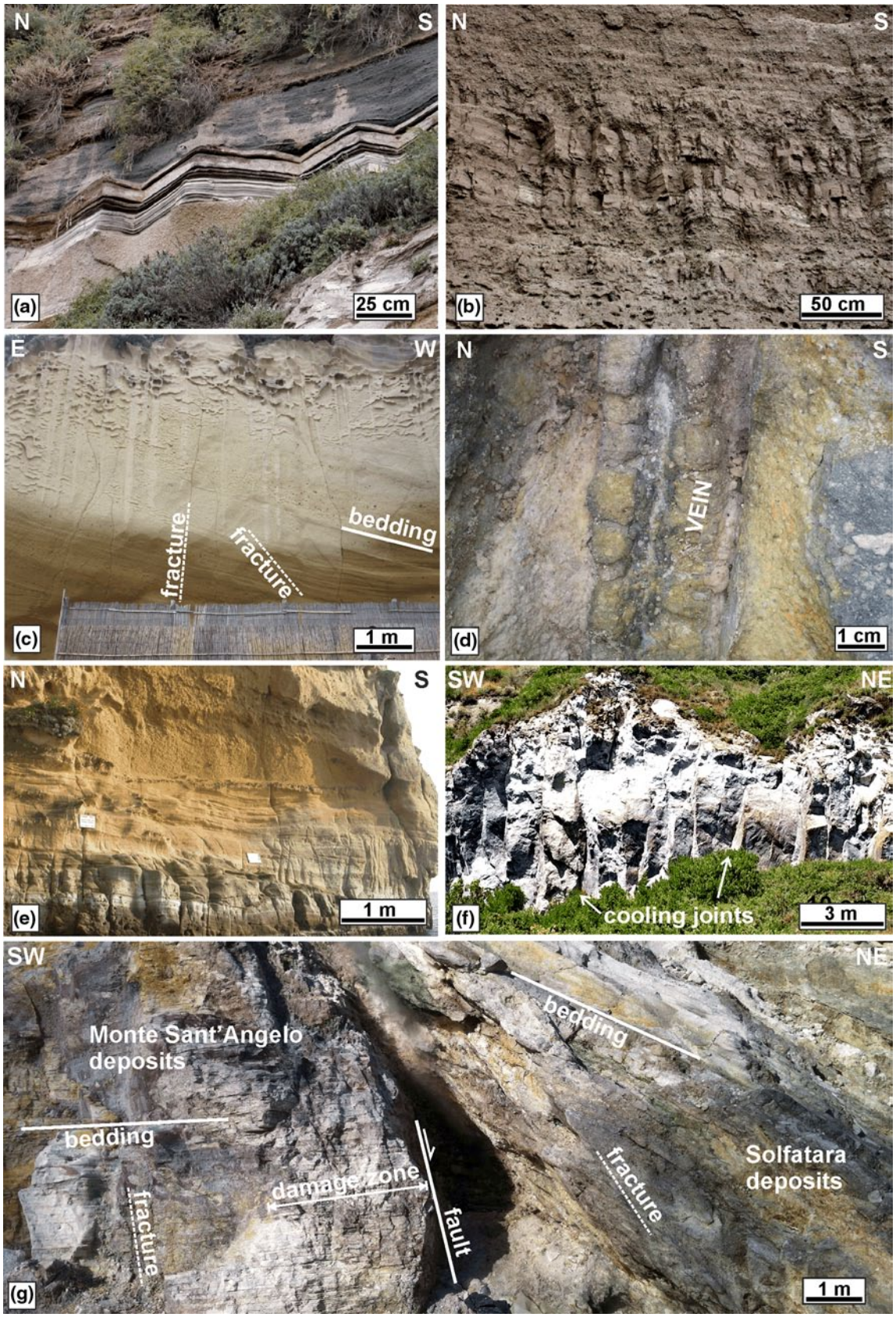
N
S
(a)
25 cm
N
S
(b)
50 cm
E
W
fracture
fracture
bedding
(c)
1 m
N
S
VEIN
(d)
1 cm
N
S
(e)
1 m
SW
NE
cooling joints
(f)
3 m
SW
NE
Monte Sant'Angelo deposits
bedding
bedding
damage zone
fault
fracture
fracture
Solfatara deposits
(g)
1 m

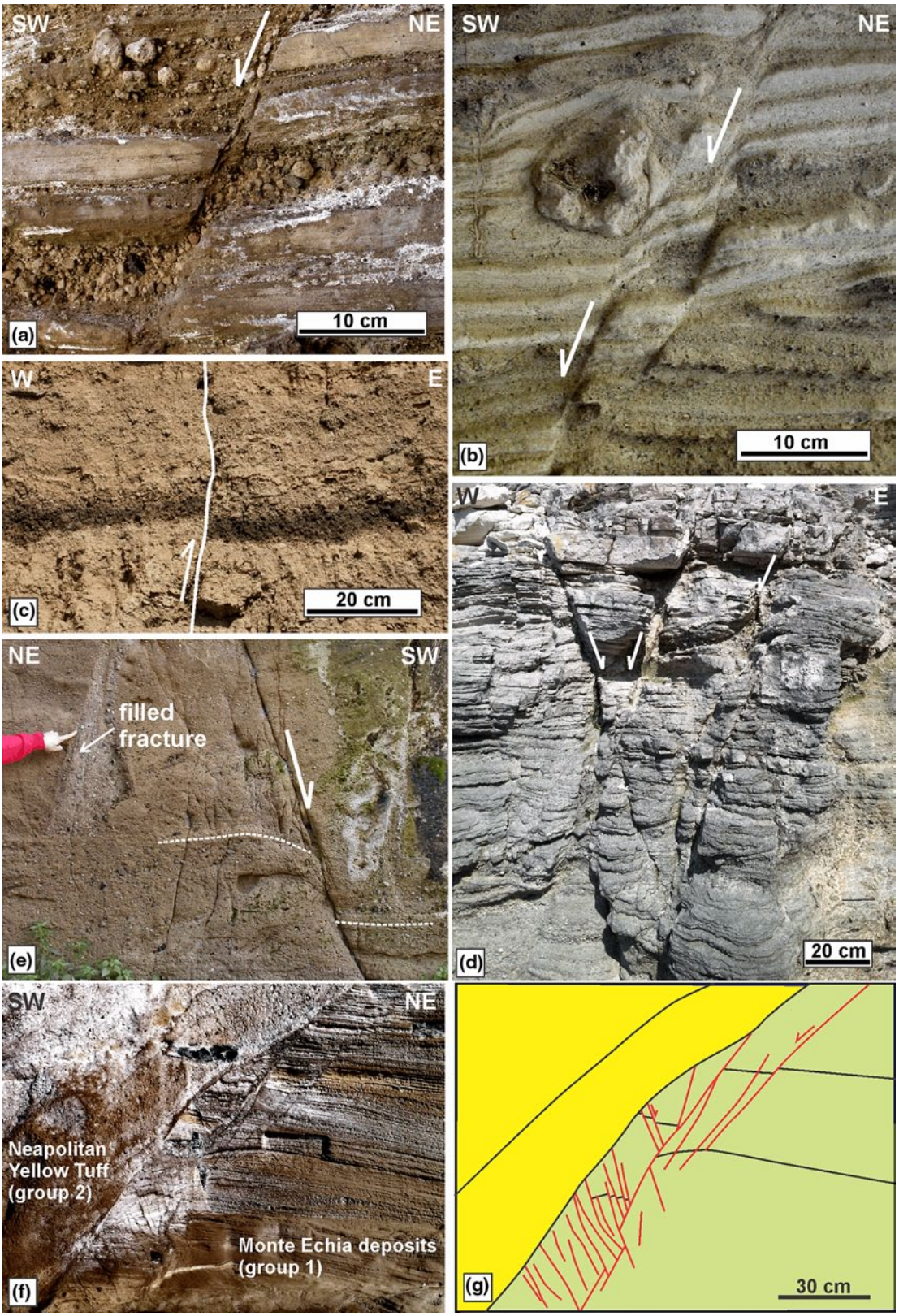

Fig. 5 Some examples of faults in volcanic rocks. **a** Normal fault, Monte Echia (*group 1*). **b** Normal faults deflecting volcanic layers, Parco Grifeo1 (*group 1*). **c** Reverse fault, Monte di Procida cliff (*group 1*). **d** Conjugate normal faults in Agnano-Monte Spina deposits (*group 3*), Solfatara1. **e** Normal fault and filled fracture in NYT (*group 2*), Casalanno1. **f** Main normal fault with several antithetic structures in Monte Echia tuff (*group 1*) sealed by massive NYT (*group 2*), Castel dell'Ovo. **g** Line drawing of the previous picture

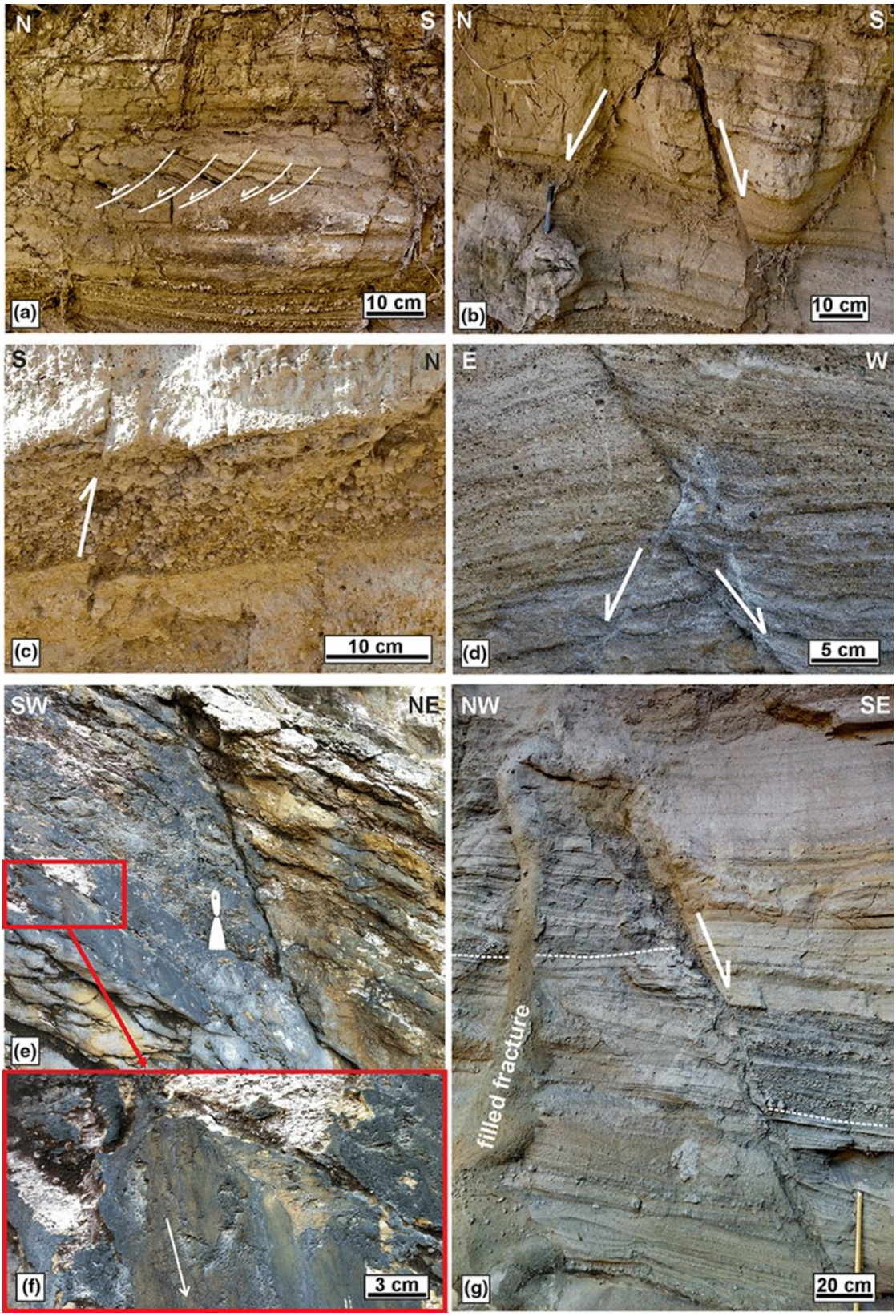

Fig. 6 Some examples of faults in volcanic rocks (*group 3*). Terme di Agnano: **a** syn-eruption listric domino normal faults; **b** conjugate normal faults. **c** Reverse fault, Cigliano1. **d** Conjugate normal faults, La Pietra. **e** Normal fault showing striations, Solfatara deposits, Pisciarelli2. **f** Zoom of previous picture. **g** Normal fault and filled fracture in Astroni deposits, Cigliano4

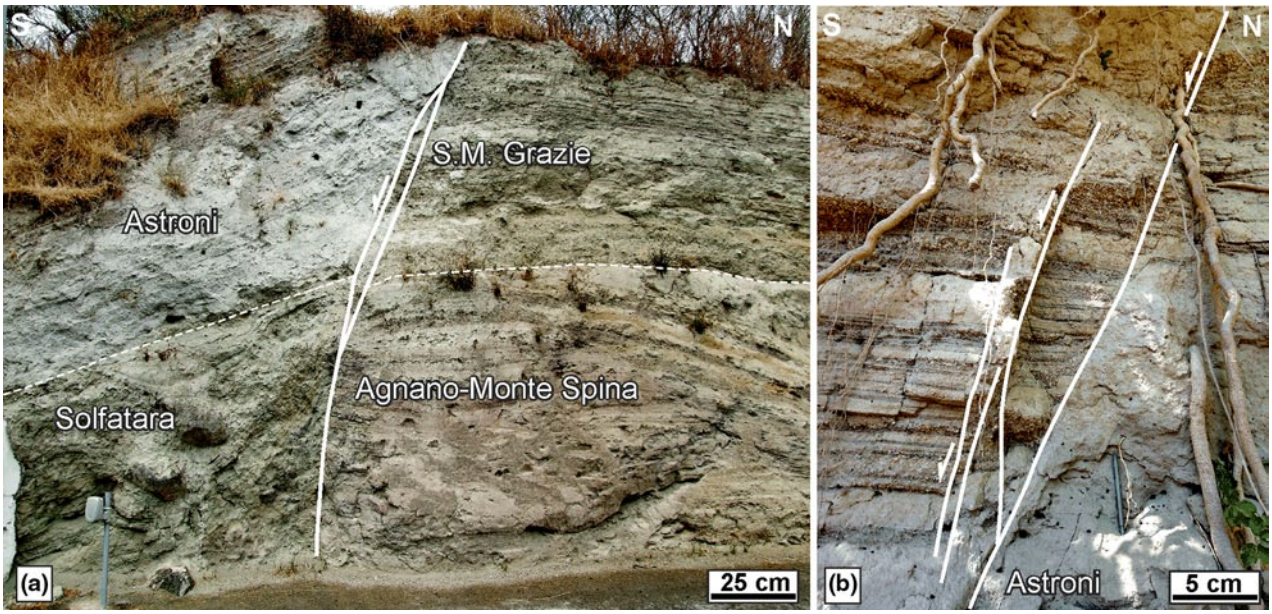

Fig. 7 Normal faults cutting *Astroni* deposits, Via Antiniana

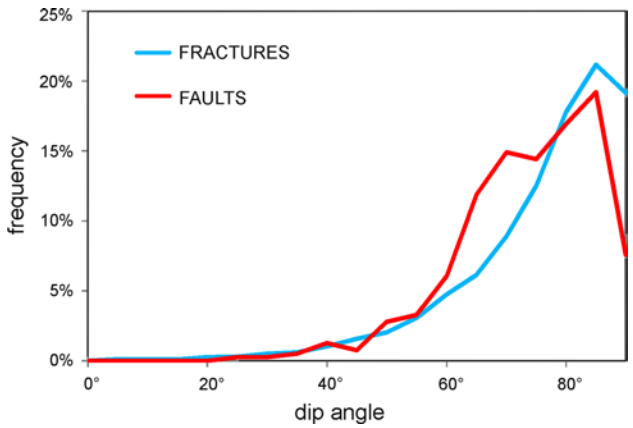

Fig. 8 Frequency histogram of *fault* and *fracture* dip angles

orthogonal to the layering ending against bedding surfaces (Fig. 4a, b, e), whereas in homogeneous deposits such as the NYT, fractures show metric lengths and spacing of several meters and vertical to moderately dipping attitudes (Fig. 4c). The naked-eye evaluation of fracture intensity indicates that this feature is highly variable: in centimeter-grained and weakly lithified rocks (e.g., pumiceous deposits), it shows very low values (1–5 fractures per meter); on the contrary, fine-grained rocks such as lithified ashes can show high values of density (up to 150 fractures per meter; Fig. 4a, b, e, g). It is very common to see alternating layers showing contrasting fracture density values (Fig. 4a, b, e). In order to estimate the fracture density variability, a statistical analysis, by means of the scan line method, was carried out across a main ring fault bounding the Agnano

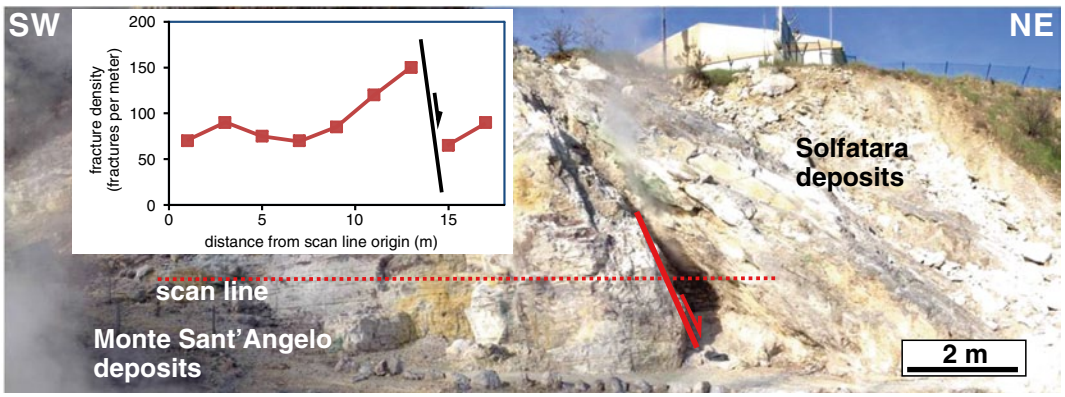

Fig. 9 Scan line (marked by a *dotted line*) drawn across a main ring fault bounding the Agnano caldera (Pisciarelli1). The *inset* shows the frequency diagram of calculated fracture density

caldera (Fig. 4g). Here, 2-m-thick damage zone is hosted in the footwall of a normal fault. The fracture density, calculated across a 17-meter-long scan line (Fig. 9), shows values from 60 to 100 fractures per meter away from the fault zone, up to 150 fractures per meter in the damage zone. In the same outcrop (Fig. 4g), moderately dipping fractures occur in the Solfatara deposits, often evolving into normal faults with small displacements (Fig. 6e, f). This kind of fractures usually occurs also in other outcrops characterized by moderately to steeply dipping strata. Other types of fractures include (1) cooling joints, hosted in massive lava deposits and characterized by a uniform fracture spacing (e.g., Fig. 4f), (2) non-conventional fractures (sensu Price and Cosgrove 1990) related to the anthropic activity, such as mining, often showing by a non-planar geometry, and (3) neo-formed fractures related to slope instability. The (2) and (3) fracture types were not considered in the following analysis.

The most of analyzed faults (Figs. 5a, b, d, e, f, 6a, b, d, e, g) show dip angles exceeding 60° (Fig. 8) generally forming conjugate sets with a conjugation angle (2θ) ranging between 10° and 60°. A dominant dip-slip kinematics for all analyzed structure can be assumed according to: (1) occasional striated surfaces (slickensides) (Fig. 6e, f); (2) occurrence of conjugate faults showing sub-horizontal intersection lines (e.g., Figs. 5d, f, 6b, d), indicating that the slip was parallel to the fault dip line (e.g., Ragan 2009); (3) occurrence of fault-related brittle–ductile deformation such as drag folds or deflexed layers (Fig. 5b) characterized by sub-horizontal fold axes. Furthermore, ductile structures associated with faults in weakly lithified volcanic sediments record deformation synchronous with volcanic eruption. An example is shown in the Fig. 6a, where syn-sedimentary listric normal faults, detached on the same layer, generated domino structures sealed by sediments related to the same volcanic event. Other syn-sedimentary structures are fault-related tensile fractures

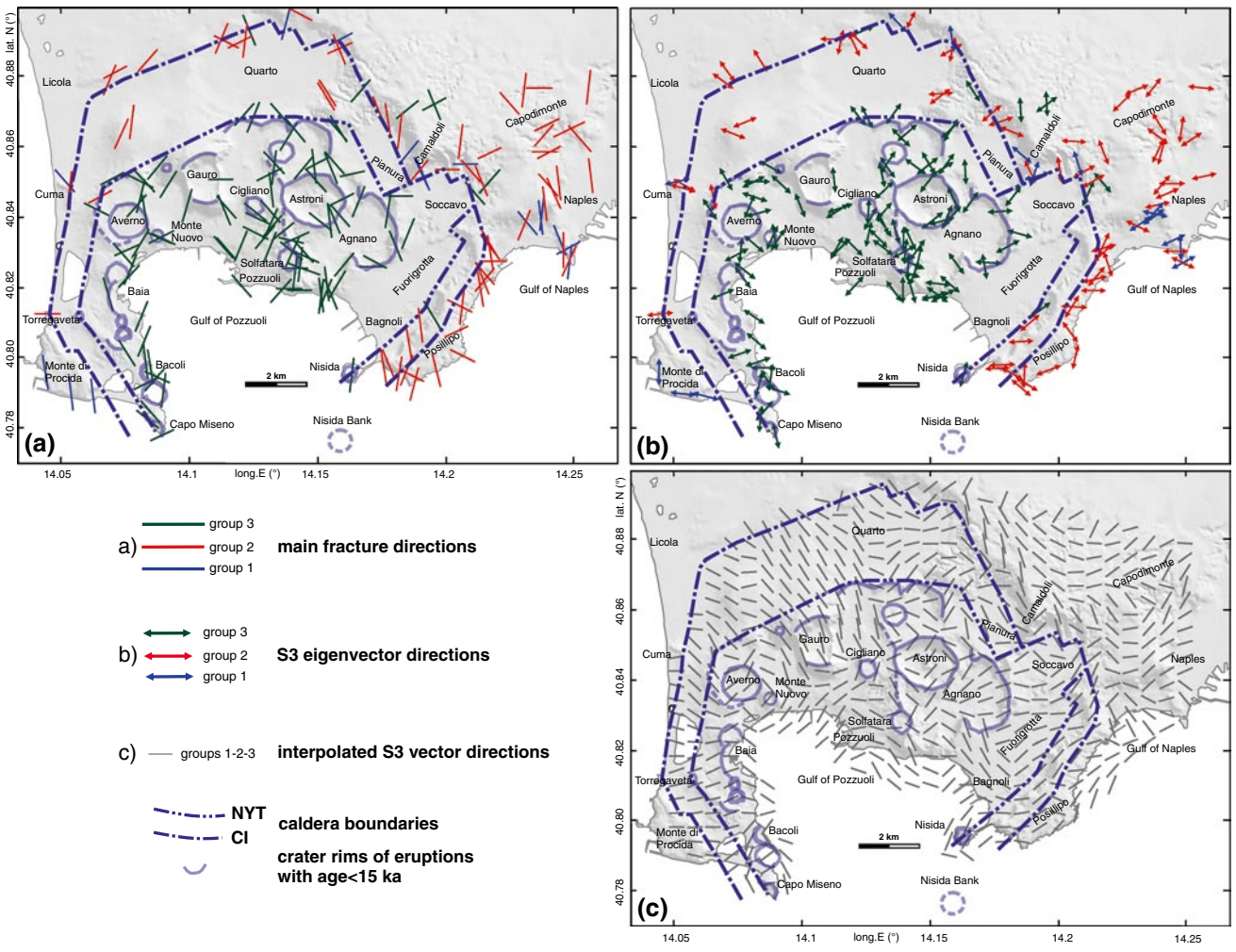

Fig. 10 **a** Map of the main fracture directions for each measurement site according to different groups. **b** Map of the S_3 vector directions such as resulting from the Bingham analysis. **c** Interpolated map of S_3 vector directions

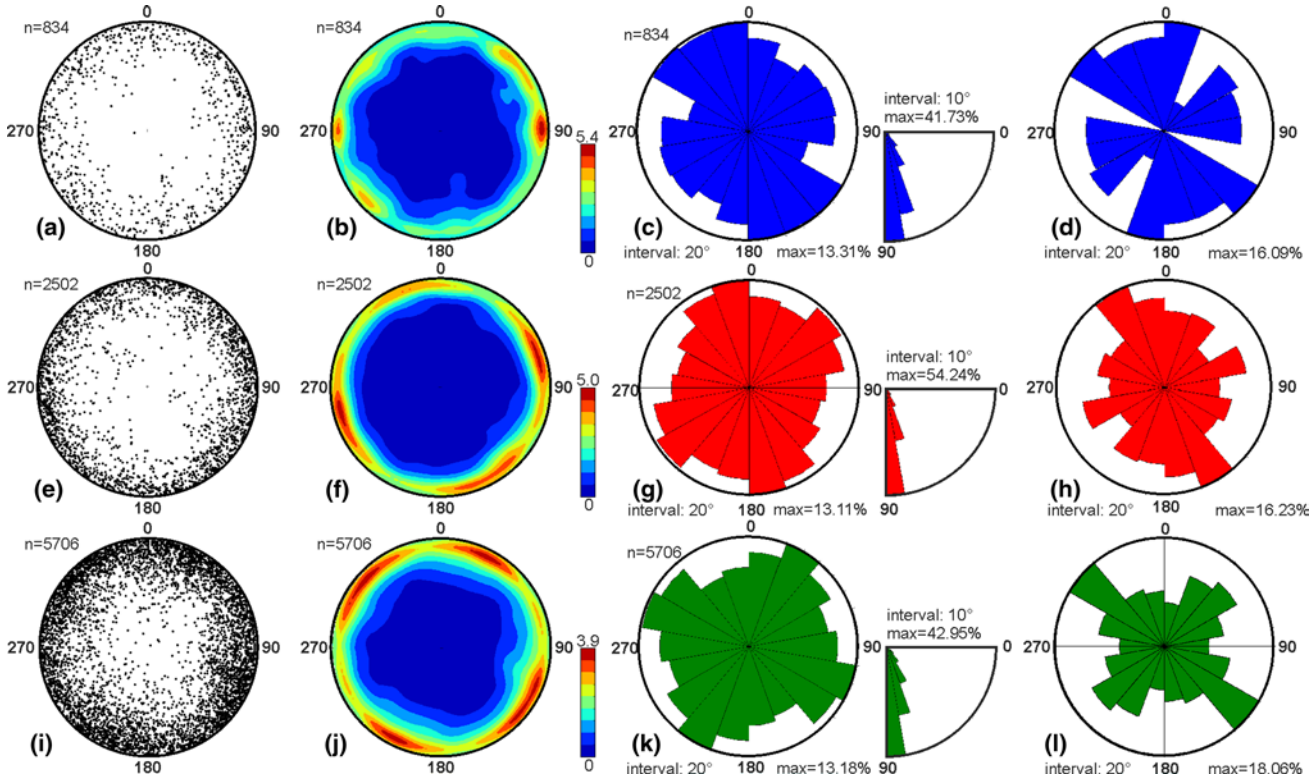

Fig. 11 Stereographic projections of poles to fractures (lower hemisphere, equiareal net), corresponding contour plots and rose diagrams of fracture direction (bidirectional) and dip: **a–c** group 1; **e–g** group 2 and **i–k** group 3. Rose diagrams of main fracture directions: **d** group 1; **h** group 2 and **l** group 3

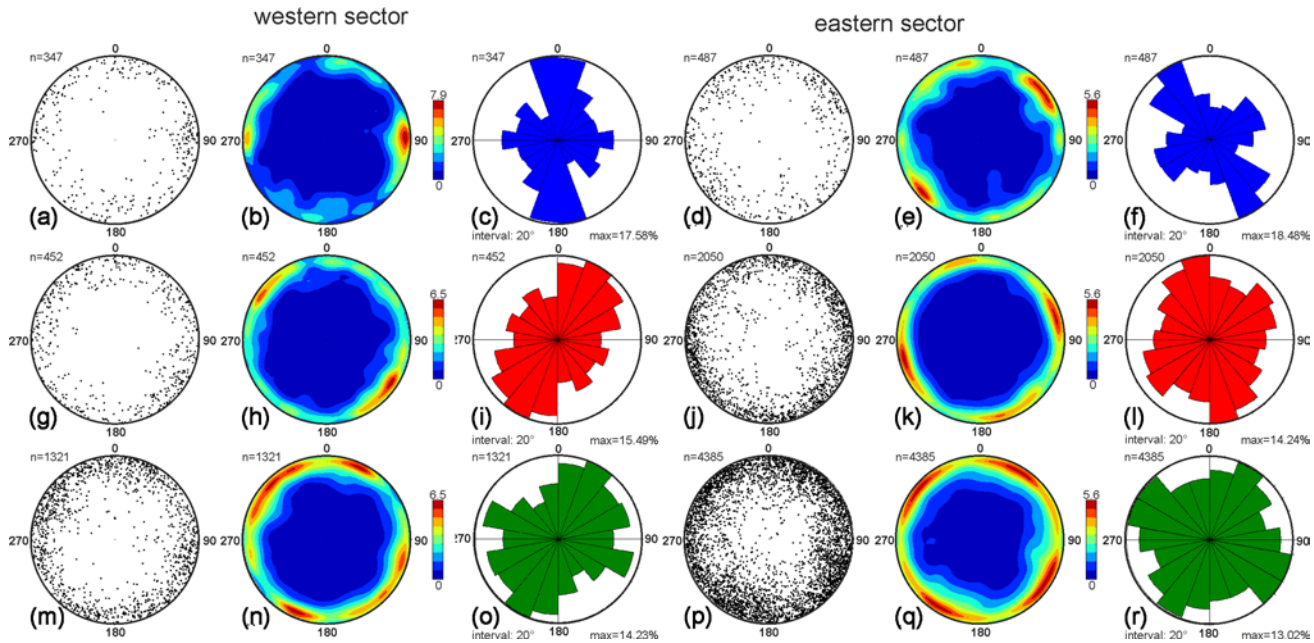

Fig. 12 Stereographic projections of poles to fractures (lower hemisphere, equiareal net), corresponding contour plots and rose diagrams of fracture directions. Western sector of the study area: **a–c** group 1; **g–i** group 2 and **m–o** group 3. Eastern sector: **d–f** group 1; **j–l** group 2 and **p–r** group 3

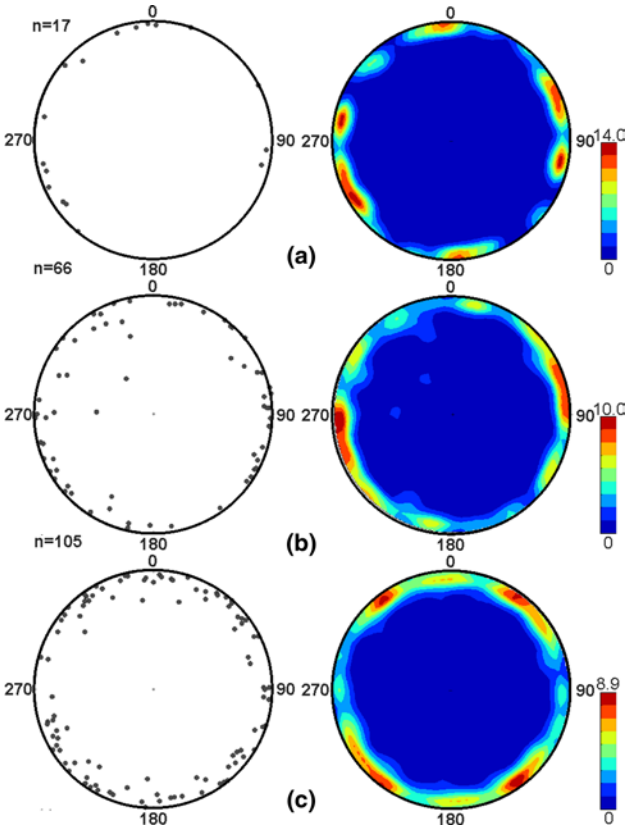

Fig. 13 Stereographic projections (lower hemisphere, equiareal net) and corresponding contour plots of the S_3 vector for: **a** group 1; **b** group 2 and **c** group 3

filled by the same volcanic sediment (Fig. 5e), while other filled fractures indicate a material injection from the bottom (e.g., Fig. 6g). For all faults, normal kinematics was dominant, even if for the almost vertical faults, occurring mainly along the caldera/crater rims, a reverse movement is not rare (Figs. 5c, 6c). The majority of analyzed faults are hosted in volcanic structures; however, some young structures are located in the central sector of caldera, between La Starza and Accademia localities (Fig. 2), often cutting the Astroni deposits and characterized by normal kinematics and centimeter to meter displacements (Figs. 6g, 7).

Orientation and paleostress analyses

Here, we present the statistical analysis of fractures and faults. Structures were analyzed by means of stereographic projections of poles to planes, relative contour plots and rose diagrams of both fracture directions and dips. In order to obtain an estimation of the extension orientation (eigenvector S_3) related to the tensile fractures, the Bingham analysis (Bingham 1974) was carried out. Further information about extension was obtained by means of P–B–T inversion method (Angelier and Mechler 1977) applied on fault data.

Fractures

A synoptic view of principal fracture directions (indicated by means of orientated lines) for all analyzed outcrops in Campi Flegrei and city of Naples is shown in the Fig. 10a. The three main fracture directions, the total number of recorded fractures, and the maximum frequency value (in percentage) of the main direction (i.e., longest rose slice of the corresponding rose diagram) are listed in the supplementary data.

Fracture data indicate a large azimuth scattering (Fig. 10a), although some trends persist for long distances, such as in the city of Naples (including the Posillipo promontory) where longitudinal directions prevail, or along the Pianura–Capodimonte lineament where the ENE–WSW direction is well recorded. In the whole area of Campi Flegrei, N30–50E and N110–130E directions are very common.

In order to analyze the relationship between fracture orientations and ages of hosting rocks, all fractures were analyzed and separated in three main groups (group 1 age $\geq$39 ka; 15 ka $\leq$ group 2 age <39 ka; group 3 age <15 ka; Fig. 11).

Fractures are generally very steep for all groups (mainly 70°–90° of dip) and characterized by the prevailing directions for the groups 1, 2, and 3 of (1) N150E; (2) N170E and N50E; (3) N30E; (4) and N110E, respectively, with a maximum frequency of ca. 13 % for all groups.

It is worth noting that fractures of groups 1 and 2 show different main directions in the western and eastern sectors of the study area (separated in Fig. 2 by a dotted line). For the group 1, N–S and secondarily E–W directions prevail in the western sector (Fig. 12a–c), whereas NW–SE and secondarily NE–SW directions are dominant in the eastern sector (Fig. 12d–f). This difference is observed also for the group 2 where NNE–SSW (Fig. 12g–i) and N170 (Fig. 12j–l) directions prevail in the western and eastern sectors, respectively. On the contrary, fracture frequency peaks of rose diagrams for the group 3 are very similar in both sectors (Fig. 12m, r).

In order to obtain information about the extension direction from fracture data in every measurement site, S_3 eigenvector attitudes were calculated by means of the Bingham analysis (Bingham 1974). Stereographic projections of all S_3 vectors, grouped according to the volcanic rock age hosting the fractures, were carried out (Fig. 13). For the group 1 (Fig. 13a), ENE–WSW and N–S are the main S_3 directions, similarly for the group 2 (Fig. 13b), the ENE–WSW direction is dominant, whereas for the group 3 (Fig. 13c), the NE–SW and NW–SE directions prevail. In order to obtain an overall view of all extension directions, estimated by Bingham analysis, all S_3 directions were placed in the map of analyzed area (Fig. 10b) (see supplementary data for

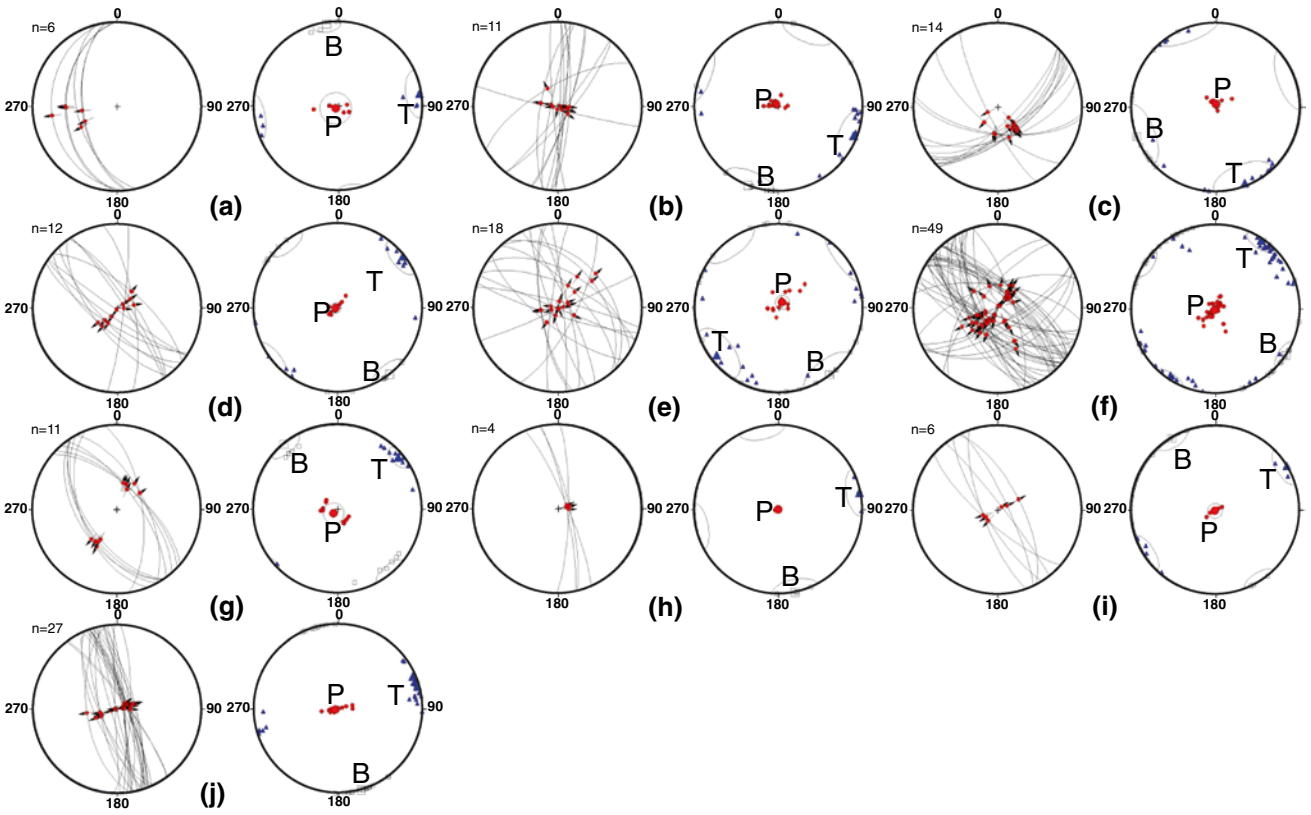

Fig. 14 Stereographic projections of recorded faults for each group (Angelier representation, lower hemisphere, equiareal net) and relative *P–B–T* plots (results are listed in the Table 1). *Group 1* **a** Acquamorta; **b** Monte di Procida; **c** Soccavo2; **d** Parco Grifeo1; **e** C.so V.E. di Savoia; **f** Monte Echia; **g** Castel dell'Ovo. *Group 2* **h** Cupa Orlando; **i** Casalanno1; **j** Lido Pola1

the S_3 vector attitude in every measurement site). A linear interpolation of data was carried out using a 30 × 30 grid (Fig. 10c).

Faults

The most of fault planes show N–S, E–W, NW–SE, and NE–SW main directions (Figs. 14, 15). Usually faults are characterized by a normal movement, whereas steeply dipping faults can show also a reverse kinematics. In order to obtain information about the paleostress regime, the P–B–T technique was applied to fault data including reactivated and neo-formed structures. This method provides the three strain axis directions for each individual fault (plane orientation, slip orientation, and kinematics): *P* (maximum shortening), *T* (maximum stretching), and *B* (intermediate axis, orthogonal to the *P–T* plane). The orientation of each strain axis was calculated using a defined fracture angle θ. Analyses were done using the software TectonicsFP 1.75.1166 (Reiter and Acs 1996–2013), which allows calculation of the best-fit angle θ minimizing the sum of all misfit angles between the measured slip direction and the maximum calculated shear stress.

The paleostress analysis invariably shows a vertical maximum shortening (*P*) and a variable sub-horizontal extension (*T*) (Table 1; Figs. 14, 15). Calculated best-fit angle θ shows an almost Gaussian frequency distribution characterized by a mean value of 20° (Fig. 16).

It is worth to note as the youngest normal faults located between La Starza and Accademia (Fig. 2), characterized always by normal kinematics and centimeter up to metric displacements (Figs. 6g, 7), indicate a constant NNE–SSW extension such as resulting by the *P–B–T* inversion (Fig. 15h, x).

Discussion

Several meso-scale faults are characterized by high dip angles (Fig. 8), suggesting that some of them can be the reactivation of inherited structures such as tensile fractures generally showing steep or vertical attitudes (Figs. 8, 11). Such high dip angles are inconsistent with those of normal faults formed in the shallow crust levels (Anderson 1905), generally characterized by dip angles of 60°. Furthermore, θ angle, i.e., the angle forming the principal stress S_1 with

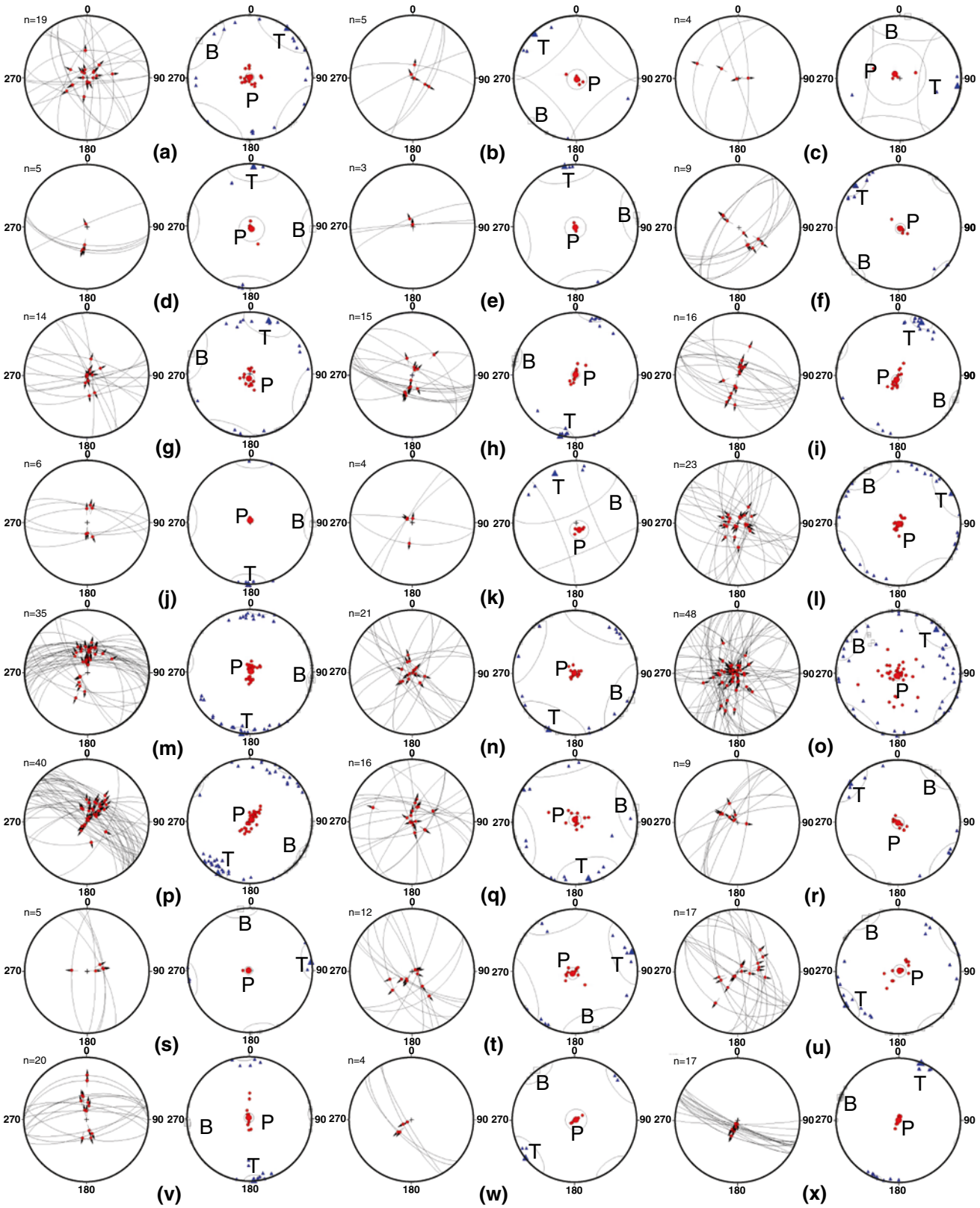

Fig. 15 Stereographic projections of recorded faults for each group (Angelier representation, lower hemisphere, equiareal net) and relative *P–B–T* plots (results are listed in the Table 1). *Group 3* **a** La Schiana; **b** Punta Epitaffio; **c** Bacoli2; **d** Bacoli6; **e** Bacoli3; **f** Starza3; **g** Cigliano1; **h** Cigliano4; **i** Cigliano2; **j** Cigliano5; **k** Senga2; **l** Solfatara Nord2; **m** Hotel Gli Dei; **n** Solfatara Nord1; **o** Solfatara Sud; **p** Pisciarelli2; **q** Pisciarelli1; **r** Via P. S. Gennaro1; **s** Astroni8; **t** La Pietra; **u** Nisida; **v** Terme di Agnano; **w** Bagnoli Futura2; **x** Via Antiniana

Table 1 List of numerical results of *P–B–T* analysis on fault data shown in the Figs. 14 and 15

Site	Group	*n*	*P*	%	*B*	%	*T*	%	*θ*°
Acquamorta	1	6	229/86	95	352/03	98	081/04	94	42
Monte di Procida	1	11	276/88	99	188/00	98	098/03	98	12
Soccavo Arin2	1	14	356/87	99	250/00	78	159/05	69	28
Parco Grifeo1	1	12	262/88	99	142/00	90	052/02	88	14
C.so V.E. di Savoia	1	18	032/84	96	143/00	68	233/07	64	16
Monte Echia	1	49	223/88	98	123/00	71	033/02	70	20
Castel dell'Ovo	1	11	225/84	95	320/00	92	050/06	96	34
Cupa Orlando	2	4	258/89	100	168/00	98	078/02	98	11
Casalanno1	2	6	230/89	99	328/00	97	058/01	96	16
Lido Pola1	2	27	252/87	99	164/00	98	074/03	96	14
La Schiana	3	19	322/89	97	306/00	41	036/00	39	20
Punta Epitaffio	3	5	152/88	98	227/00	75	317/02	73	14
Bacoli2	3	4	310/82	88	007/00	89	097/08	77	22
Bacoli6	3	5	154/85	96	093/00	95	003/05	92	30
Bacoli3	3	3	194/89	99	080/00	98	350/01	97	6
Starza3	3	9	122/88	98	225/00	95	315/03	94	24
Cigliano1	3	14	190/84	97	289/00	66	019/09	65	14
Cigliano4	3	15	341/90	98	285/00	91	195/00	89	22
Cigliano2	3	16	204/84	97	113/00	93	023/07	90	24
Cigliano5	3	6	003/88	100	092/00	95	182/02	95	20
Senga2	3	4	156/80	99	067/00	72	337/14	73	20
Solfatara Nord2	3	23	197/89	99	329/00	45	059/01	44	16
Hotel Gli Dei	3	35	074/89	98	098/00	84	188/01	82	26
Solfatara Nord1	3	21	314/89	99	132/00	51	222/01	51	10
Solfatara Sud	3	48	214/86	89	304/04	17	049/08	13	10
Pisciarelli2	3	40	049/87	97	122/00	84	212/03	81	18
Pisciarelli1	3	16	342/86	95	076/00	45	167/09	43	18
Via P. S. Gennaro1	3	9	173/89	98	039/00	88	309/01	86	18
Astroni8	3	5	269/88	100	351/00	97	081/01	96	20
La Pietra	3	12	231/85	97	161/00	57	070/04	54	18
Nisida	3	17	055/88	94	328/00	83	238/02	78	24
Terme di Agnano	3	20	338/89	96	266/00	96	176/01	92	26
Bagnoli Futura2	3	4	079/88	98	323/00	98	233/02	96	18
Via Antiniana	3	17	239/90	99	291/00	98	021/00	97	10

the fault plane, such as resulting from the *P–B–T* analysis (Fig. 16), shows frequently values <30° with a mean value of 20°. These types of faults are very common in volcanic settings (e.g., Gudmundsson 1987) and have been observed also in several analogical experiments (see Acocella 2007 for a review). According to Hardy (2013) such faults, characterized by steep planes and low conjugation angles, can form as response of a footwall collapse related to a normal faulting in the basement (Fig. 18), such as resulting in the caldera/crater formation. In such a model, steep tensile fractures, formed along the topographic surface, join with upward propagating normal faults enucleated in the basement.

Some analyzed faults can be considered as ring faults bounding the caldera planes such as the structure shown in the Fig. 4g located in the Pisciarelli outcrop along the western rim of Agnano caldera. This fault has formed a 2-meter-thick damage zone in the footwall with a fracture density increasing from the host rock toward the fault plane (Fig. 9). At larger scale only, some faults indicate extension about orthogonal to the CI and NYT caldera rims (Fig. 17), whereas others, such as for the Nisida and Bagnoli areas (Fig. 2), provide extensions about parallel to the SE caldera edge. Other faults, such as those located between Baia and Punta Epitaffio (Fig. 2), indicate meridian and longitudinal extensions (Fig. 17) without a clear relationship with the SW edge of the CI caldera. Outside of CI caldera meridian, extensions are recorded in the Monte di Procida cliff (Fig. 17) whereas NE–SW extension prevails in the city of Naples.

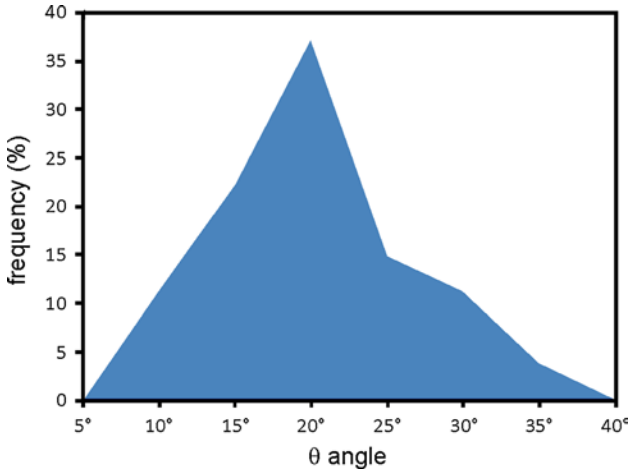

Fig. 16 Frequency histogram of θ angles such resulted from the *P–B–T* analysis

Meso-scale faults occurring close to the volcanic edifices (e.g., Monte di Procida, Monte Echia, Nisida, Agnano, Fig. 2) are frequently associated with brittle–ductile structures suggesting a syn-eruption deformation. The brittle deformation in the NYT exposures is very scarce, with faults observed only in few places such as the Casalanno and Posillipo areas located along the NE and SE border of the CI caldera, respectively (Figs. 2, 17); these rocks are far from the NYT caldera, presently buried under younger volcanic structures (Fig. 2). We propose that these rocks did not recorded the successive deformation related to the younger volcanic activity (ages <15 ka) because it was mostly localized within NYT caldera (e.g., Di Vito et al. 1999).

Meso-scale faults of group 1 (age ≥39 ka), occurring in the eastern sector (city of Naples, close to C.so V.E. di Savoia and Monte Echia, Fig. 2) and in the westernmost sector (Monte di Procida area, Fig. 2), indicate NE–SW and WSW–ENE extensions, respectively (Figs. 14, 17). These different directions of extension, for W and E sectors of the caldera (Fig. 2), are characterized by an angle of about 30° between them, the same angle measured between the fracture frequency peaks of the rose diagrams in the two sectors for groups 1 and 2 (Fig. 12c, f, i, l). This difference could result from (1) a local change of the stress field or (2) a post-NYT deformation of the westernmost sector of Campi Flegrei, probably as consequence of the resurgence of the central sector of the caldera.

Further information on stress field resulted from Bingham and *P–B–T* analyses carried out on fracture and fault data, respectively. The stereographic projections of S_3 eigenvectors (Fig. 13) indicate that the stress field was similar for fracture development hosted in rocks of groups 1 and 2 (age ≥15 ka) characterized by an about main ENE–WSW extension (Fig. 13a, b). On the other hand, the stress field related to the fractures in younger rocks (age <15 ka) was characterized by two main NE–SW and NW–SE extensions (Fig. 13c).

The occurrence of two mutually orthogonal fracture sets can be a consequence of a local exchange between intermediate (σ_2) and minimum (σ_3) stress axes close to the growing fractures, without invoking a rotation of the remote stress field (Caputo 1995). However, also at regional scale, two orthogonal fault sets (characterized by NW–SE and NE–SW directions, respectively) are widely present (e.g., Fig. 1). The NW–SE "Apennine" faults are generally considered as associated with the Tyrrhenian back-arc opening from the Middle Tortonian to the Present (e.g., Vitale and Ciarcia 2013 and references therein), whereas the NE–SW "anti-Apennine" structures are interpreted as (1) transfer faults connecting NW–SE planes (e.g., Acocella et al. 1999) or (2) normal faults related to the Pliocene–Quaternary opening of the Marsili Basin, located southward of the study area (e.g., Casciello et al. 2006). The occurrence of a secondary extension in several outcrops close to the eruption vents results also from the *P–B–T* analysis (Figs. 14, 15). The occurrence of steep faults with a general normal and occasional reverse kinematics within a radial normal stress regime well fit with the caldera/crater collapse models described by several authors (among others Geyer and Martì 2008; Acocella 2008 and reference therein).

The moderate dispersion of fracture directions, observed in the most of sites, can be related to local effects on the stress field as consequence of (1) heterogeneity and anisotropy of the host rocks and (2) successive deformations associated with the younger volcano-tectonic processes among other dome resurgence phenomena (Vilardo et al. 2010). On the other hand, the slight prevalence of "Apennine" (NW–SE) and "anti-Apennine" (NE–SW) trends, such as resulting both from the fracture direction (Fig. 11) and S_3 vector (Fig. 13) analyses, suggests that the control on fracture distribution by a regional stress field is partially covered by local stress fields. All these features indicate a complex strain evolution strictly related to the sequence of eruptive events, which probably led to a strongly change in the previous "regional" structure orientations following significant deformation phases related to the major eruptions. Furthermore, it should be stressed as the youngest faults, localized in the central sector of caldera, indicate a NNE–SSW extension probably related to the very recent uplift phenomena characterized by maximum values of vertical and horizontal ground velocities in the Pozzuoli (Fig. 2) and the area between La Starza and Accademia, respectively (Vilardo et al. 2010).

The kinematic and orientation analyses carried out from this study on faults and fractures hosted in the volcanic rocks of Campi Flegrei suggest a caldera development

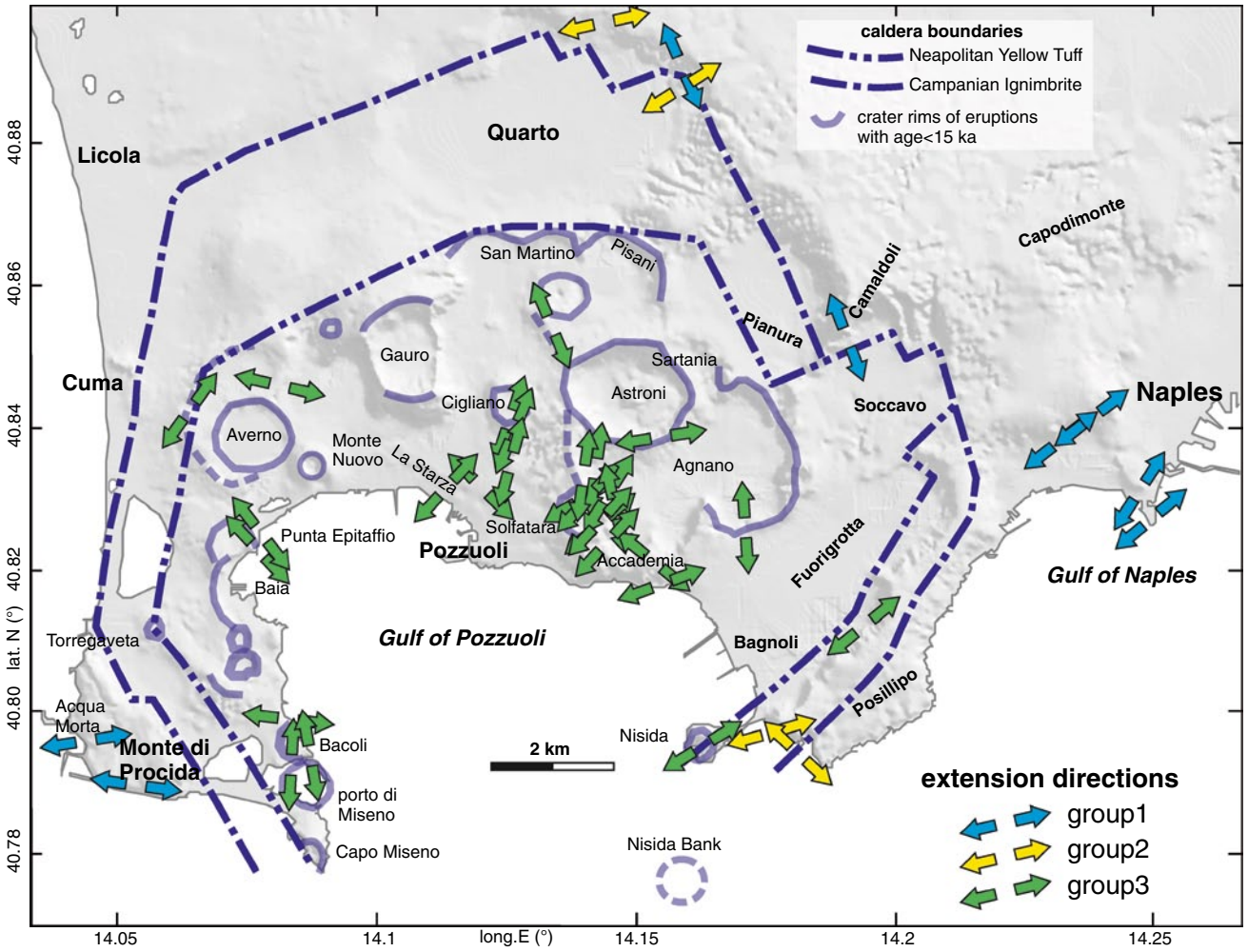

Fig. 17 Map of extension directions (*T* axis trends) resulting from the *P*–*B*–*T* analysis

strongly controlled by preexisting structures. According to experiments on the influence of inherited planar structures on the caldera formation (e.g., Holohan et al. 2005), we envisage a piecemeal model (Fig. 19) characterized by a polygonal caldera outline in good agreement for both the ca. 12-km-wide CI caldera and the smaller calderas/craters (Fig. 2). The piecemeal collapse has the inherited NW–SE, NE–SW, and secondarily N–S and E–W fractures, which exerted a strong control on the dynamics of the caldera evolution. Caldera/crater collapse reactivated steep planar structures previously formed in response to both the regional extensional regime and local deformation related to a resurgent dome. These fractures, turned in faults with normal and secondarily reverse kinematics, were formed before or during the eruption and allowed the development of a caldera with a quite rounded segmented rim (Fig. 19).

Conclusions

The detailed structural analysis of fractures and faults in Campi Flegrei and city of Naples allowed the reconstruction of a complex strain pattern characterized by deformation structures formed in different stages of the volcanic history. Normally, tensile fractures appear in two mutually orthogonal sets, generally both being orthogonal to the volcanic bedding. The fracture density is highly variable with an increase close to the main fault bounding caldera/crater rims. Recorded faults include both very steep and moderately dipping conjugate planes, most of them with normal kinematics. Ductile deformation, such as that expressed by drag folds or deflexed layers, is associated with syn-eruption faults growth. The widespread lack of faults within the NYT deposits suggests that the exposed NYT deposits are

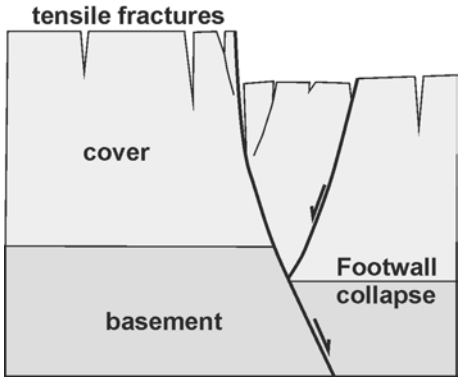

Fig. 18 Model of conjugate steep normal faults associated to the caldera/crater collapse (from Hardy 2013; modified)

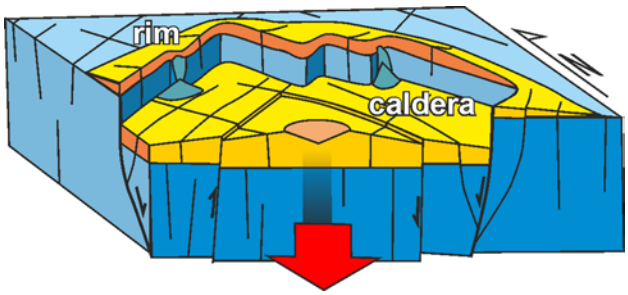

Fig. 19 Piecemeal caldera collapse controlled by inherited structures

far from the caldera rim, presently buried under younger volcanic rocks of Campi Flegrei.

The fracture direction analysis indicates that the study area is characterized by a large dispersion of planar trends, with some sectors showing preferred orientations. In some cases, fractures are parallel or orthogonal to the caldera boundaries, but in the most of cases, the main fracture directions indicate a complex interaction between caldera development and the "regional" stress regime. According to their spatial distribution, fractures of groups 1 and 2 show preferred orientations differing of ca. 30° for the western and eastern sectors of the investigated area. On the contrary, younger fractures (group 3) show a prevalence of "Apennine" (NW–SE) and "anti-Apennine" (NE–SW) directions. Youngest normal faults within the central sector of caldera indicate a local NNE–SSW extension probably related to the resurgence phenomena. Many of the recorded fractures and faults played an important role reactivating during the volcano-tectonic processes leading to the formation of both main piecemeal caldera structure of Campi Flegrei and small size calderas and craters.

Acknowledgments We thank the topic editor Christoph Breitkreuz and the reviewer Francesco Mazzarini for the extremely useful comments and suggestions that significantly improved this paper. Special thanks to Francesco D'Assisi Tramparulo, Carlo Scirocco, and Enrico Iannuzzi for the help in the field work and, finally, to Mauro Rosi for the interesting discussions. This work was partly funded by the Italian Department of Civil Defence Protection within framework DPC-INGV 2012-2021, Volcanological Project V1.

References

Acocella V (2007) Understanding caldera structure and development: an overview of analogue models compared to natural calderas. Earth-Sci Rev 85:125–160

Acocella V (2008) Activating and reactivating pairs of nested collapses during caldera forming eruptions: Campi Flegrei (Italy). Geophys Res Lett 35:L17304. doi:10.1029/2008GL035078

Acocella V (2010) Evaluating fracture patterns within a resurgent caldera: Campi Flegrei, Italy. Bull Volcanol 72:623–638

Acocella V, Salvini F, Funiciello R, Faccenna C (1999) The role of transfer structures on volcanic activity at Campi Flegrei (southern Italy). J Volcanol Geotherm Res 91:123–139

Anderson EM (1905) The dynamics of faulting. Trans Edinb Geol Soc 8:387–402

Angelier J, Mechler P (1977) Sur une methode graphice de recherche des contraintes principales egalement utilisable en tectonique et en seismologie: la methode des diedres droits. Bulletin Societé Geologique France XIX(7):1309–1318

Arienzo I, Moretti R, Civetta L, Orsi G, Papale P (2010) The feeding system of Agnano–Monte Spina eruption (Campi Flegrei, Italy): dragging the past into present activity and future scenarios. Chem Geol 270(1–4):135–147

Barberi F, Corrado G, Innocenti F, Luongo G (1984) Phlegraean Fields 1982–1984: brief chronicle of a volcano emergency in a densely populated area. Bull Volcanol 47(2):175–185

Barberi F, Carapezza M, Innocenti F, Luongo G, Santacroce R (1989) The problem of volcanic unrest: the Phlegraean Fields case history. Atti Conv Lincei 80:387–405

Battaglia M, Troise C, Obrizzo F, Pingue F, De Natale G (2006) Evidence for fluid migration as the source of deformation at Campi Flegrei caldera (Italy). Geophys Res Lett 33:L01307–L013010. doi:10.1029/2005GL024904

Berrino G, Corrado G, Luongo G, Toro B (1984) Ground deformation and gravity change accompanying the 1982 Pozzuoli uplift. Bull Volcanol 47(2):187–200

Bingham C (1974) An antipodally symmetric distribution on the sphere. Ann Stat 2:1201–1225

Bodnar R, Cannatelli C, De Vivo B, Lima A, Belkin H, Milia A (2007) Quantitative model for magma degassing and ground deformation (bradyseism) at Campi Flegrei, Italy. Geology 35:791–794

Bruno PPG, Rapolla A, Di Fiore V (2003) Structural setting of the Bay of Naples (Italy) seismic reflection data: implications for Campanian volcanism. Tectonophysics 372:193–213

Calcaterra D, Gianni A, Ietto A, Pappone G (1988) Sistemi di fratturazione nei tufi post-calderici dell'area flegrea. Mem Soc Geol Italy 41:936–940

Caputo R (1995) Evolution of orthogonal sets of coeval extension joints. Terra Nova 7:479–490

Casciello E, Cesarano M, Pappone G (2006) Extensional detachment faulting on the Tyrrhenian margin of the southern Apennines contractional belt (Italy). J Geol Soc Lond 163:617–629

Chiodini G, Caliro S, De Martino P, Avino R, Gherardi F (2012) Early signals of new volcanic unrest at Campi Flegrei caldera? Insights from geochemical data and physical simulations. Geology 40:943–946

Cinque A, Patacca E, Scandone P, Tozzi M (1993) Quaternary kinematic evolution of the southern Apennines. Relationships between surface geological features and deep lithospheric structures. Ann Geophys 36:249–260

Civetta L, Orsi G, Pappalardo L, Fisher R, Heiken G, Ort M (1997) Geochemical zoning, mingling, eruptive dynamics and depositional processes—the Campanian Ignimbrite, Campi Flegrei caldera, Italy. J Volcanol Geotherm Res 75:183–197

Cosentino D, De Rita D, Funicello R, Parotto M, Salvini F, Vittori E (1984) Fracture system in Phlegraean Fields (Naples, southern Italy). Bull Volcanol 47(2):247–257

Costa A, Folch A, Macedonio G, Giaccio B, Isaia R, Smith V (2012) Quantifying volcanic ash dispersal and impact of the Campanian Ignimbrite super-eruption. Geophys Res Lett 39:L10310. doi:10.1029/2012GL051605

de Vita S, Orsi G, Civetta L, Carandente A, D'Antonio M, Di Cesare T, Di Vito M, Fisher RV, Isaia R, Marotta E, Ort M, Pappalardo L, Piochi M, Southon J (1999) The Agnano–Monte Spina eruption (4.1 ka) in the resurgent, nested Campi Flegrei caldera (Italy). J Volcanol Geotherm Res 91:269–301

De Vivo B, Rolandi G, Gans PB, Calvert A, Bohrson WA, Spera FJ, Belkin AE (2001) New constraints on the pyroclastic eruption history of the Campanian volcanic plain (Italy). Mineral Petrol 73:47–65

Deino AL, Orsi G, Piochi M, de Vita S (2004) The age of the Neapolitan Yellow Tuff caldera-forming eruption (Campi Flegrei caldera–Italy) assessed by $^{40}Ar/^{39}Ar$ dating method. J Volcanol Geotherm Res 133:157–170

Del Gaudio C, Aquino I, Ricciardi GP, Ricco C, Scandone R (2010) Unrest episodes at Campi Flegrei: a reconstruction of vertical ground movements during 1905–2009. J Volcanol Geotherm Res 185:48–56

Di Renzo V, Arienzo I, Civetta L, D'Antonio M, Tonarini S, Di Vito MA, Orsi G (2011) The magmatic feeding system of the Campi Flegrei caldera: architecture and temporal evolution. Chem Geol 281:227–241

Di Vito MA, Isaia R, Orsi G, Southon J, de Vita S, D'Antonio M, Pappalardo L, Piochi M (1999) Volcanism and deformation since 12000 years at the Campi Flegrei caldera (Italy). J Volcanol Geotherm Res 91:221–246

Dvorak JJ, Gasparini P (1991) History of earthquakes and vertical ground movement in Campi Flegrei caldera, Southern Italy: comparison of precursory events to the A.D. 1538 eruption of Monte Nuovo and of activity since 1968. J Volcanol Geotherm Res 48:77–92

Fisher RV, Orsi G, Ort M, Heiken G (1993) Mobility of a large-volume pyroclastic flow-emplacement of the Campanian ignimbrite, Italy. J Volcanol Geotherm Res 56:205–220

Florio G, Fedi M, Cella F, Rapolla A (1999) The Campanian Plain and Phlegrean Fields: structural setting from potential field data. J Volcanol Geotherm Res 91:361–379

Geyer A, Martì J (2008) The new worldwide collapse caldera 232 database (ccdb): a tool for studying and understanding caldera processes. J Volcanol Geotherm Res 175:334–354

Giaccio B, Isaia R, Fedele F, Di Canzio E, Hoffecker J, Ronchitelli A, Sinitsyn A, Anikovich M, Lisitsyn S, Popov V (2008) The Campanian Ignimbriteand Codola tephra layers: two temporal/stratigraphic markers for the Early Upper Palaeolithic in southern Italy and eastern Europe. J Volcanol Geotherm Res 177:208–226

Gudmundsson A (1987) Tectonics of the Thingvellir fissure swarm, SW Iceland. J Struct Geol 9:61–69

Guidoboni E, Ciuccarelli C (2011) The Campi Flegrei caldera: historical revision and new data on seismic crises, bradyseisms, the Monte Nuovo eruption and ensuing earthquakes (twelfth century 1582 ad). Bull Volcanol 73:655–677

Hardy S (2013) Propagation of blind normal faults to the surface in basaltic sequences: insights from 2D discrete element modelling. Mar Pet Geol 48:149–159

Holohan EP, Troll VR, Walter TR, Munn S, McDonnell S, Shipton ZK (2005) Elliptical calderas in active tectonic settings: an experimental approach. J Volcanol Geotherm Res 144:119–135

Isaia R, Marianelli P, Sbrana A (2009) Caldera unrest prior to intense volcanism in Campi Flegrei (Italy) at 4.0 ka B.P.: implications for caldera dynamics and future eruptive scenarios. Geophys Res Lett 36:L21303. doi:10.1029/2009GL040513

Lirer L, Luongo G, Scandone R (1987) On the volcanological evolution of Campi Flegrei. EOS 68(16):226–234

Marianelli P, Sbrana A, Proto M (2006) Magma chamber of Campi Flegrei supervolcano at the time of eruption of the Campanian Ignimbrite. Geology 34:937–940

Milia A, Torrente MM, Giordano F (2000) Active deformation and volcanism offshore Campi Flegrei, Italy: new data from high-resolution seismic reflection profiles. Mar Geol 171:61–73

Morhange C, Marriner N, Laborel J, Todesco M, Oberlin C (2006) Rapid sea-level movements and noneruptive crustal deformation in the Phlegrean Fields caldera, Italy. Geology 34:93–96

Orsi G, D'Antonio M, de Vita S, Gallo G (1992) The Neapolitan Yellow Tuff, a large-magnitude trachytic phreatoplinian eruption: eruptive dynamics, magma withdrawal and caldera collapse. J Volcanol Geotherm Res 53:275–287

Orsi G, Di Vito M, de Vita S (1996) The restless, resurgent Campi Flegrei Nested Caldera (Italy): constraints on its evolution and configuration. J Volcanol Geotherm Res 74:179–214

Orsi G, Civetta L, Del Gaudio C, De Vita S, Di Vito MA, Isaia R, Petrazzuoli S, Ricciardi GP, Ricco C (1999) Short-term ground deformations and seismicity in the nested Campi Flegrei caldera (Italy). J Volcanol Geotherm Res 91:415–451

Orsi G, Di Vito MA, Isaia R (2004) Volcanic hazard assessment at the restless Campi Flegrei caldera. Bull Volcanol 66:514–530

Perrotta A, Scarpati C, Luongo G, Morra V (2006) The Campi Flegrei caldera boundary in the city of Naples. In: De Vivo B (ed) Volcanism in the Campania Plain: Vesuvius, Campi Flegrei and Ignimbrites. Amsterdam, Elsevier, Developments in Volcanology 9:85–96

Perrotta A, Scarpati C, Luongo G, Morra V (2010) Stratigraphy and volcanological evolution of the southwestern part of Campi Flegrei and Procida Island (Italy). In: Groppelli G, Viereck-Goette L (eds) Stratigraphy and geology of volcanic areas. Geol Soc Am Sp Paper 464:171–191

Price NJ, Cosgrove JW (1990) Analysis of geological structures. Cambridge University Press, Cambridge, p 502

Ragan DM (2009) Structural geology. An introduction to geometrical techniques. Cambridge University Press, Cambridge, p 602

Rolandi G, Bellucci F, Heizler MT, Belkin HE, De Vivo B (2003) Tectonic controls on the genesis of ignimbrites from the Campanian Volcanic Zone, southern Italy. Mineral Petrol 79:3–31

Rosi M, Sbrana A (1987) The Phlegraean Fields, Quaderni de 'La ricerca Scientifica' 114. Consiglio Nazionale delle Ricerche, Rome

Rosi M, Vezzoli L, Aleotti P, De Censi M (1996) Interaction between Caldera collapse and eruptive dynamics during the Campanian Ignimbrite eruption, Phlegrean fields, Italy. Bull Volcanol 57:541–554

Sacchi M, Alessio G, Aquino I, Esposito E, Molisso F, Nappi R, Porfido S, Violante C (2009) Risultati preliminari della campagna oceanografica CAFE_07-Leg 3 nei Golfi di Napoli e Pozzuoli, Mar Tirreno Orientale. Quaderni di Geofisica 64:1–16

Scarpati C, Cole P, Perrotta A (1993) The Neapolitan Yellow Tuff—a large volume multiphase eruption from Campi Flegrei, southern Italy. Bull Volcanol 55:343–356

Scarpati C, Perrotta A, Lepore S, Calvert A (2012) Eruptive history of Neapolitan volcanoes: constraints from 40Ar–39Ar dating. Geol Mag 150:412–425

Smith VC, Isaia R, Pearce NJC (2011) Tephrostratigraphy and glass compositions of post-15 kyr Campi Flegrei eruptions: implications for eruption history and chronostratigraphic markers. Quat Sci Rev 30:3638–3660

Vilardo G, Isaia R, Ventura G, De Martino P, Terranova C (2010) InSAR Permanent Scatterer analysis reveals fault reactivation during inflation and deflation episodes at Campi Flegrei caldera. Remote Sens Environ 114:2373–2383

Vitale S, Ciarcia S (2013) Tectono-stratigraphic and kinematic evolution of the southern Apennines/Calabria-Peloritani Terrane system (Italy). Tectonophysics 583:164–182